Available online at www.sciencedirect.com

SCIENCE DIRECT®

Bioelectrochemistry 68 (2006) 134–143

Bioelectrochemistry

www.elsevier.com/locate/bioelechem

Bioelectrocatalysis in ionic liquids. Examining specific cation and anion effects on electrode-immobilized cytochrome *c*☆

Cory M. DiCarlo, David L. Compton*, Kervin O. Evans, Joseph A. Laszlo

New Crops and Processing Technology Research Unit, United States Department of Agriculture, Agricultural Research Service, National Center for Agricultural Utilization Research, 1815 N. University St., Peoria, IL 61604 USA

Received 11 August 2004; received in revised form 28 December 2004; accepted 11 January 2005
Available online 11 July 2005

Abstract

Cytochrome *c* immobilized on alkylthiol self-assembled monolayers exhibits a characteristic Fe(II)/Fe(III) redox signal that is lost when exposed to ionic liquids composed of a butylimidazolium cation combined with either hexafluorophosphate or bis(trifluoromethylsulfonyl)imide anion. In this study it was shown that exposure to the aqueous solubilized ionic liquid components, butyl-, hexyl-, and octyl-imidazolium cations and hexafluorophosphate, tetrafluoroborate, and bis(trifluoromethylsulfonyl)imide anions, resulted in partial electrochemical signal loss. Absorbance and fluorescence measurements showed that signal loss due to the cationic ionic liquid component followed a different mechanism than that of the anionic component. Although a portion of the signal was recoverable, irreversible signal loss also occurred in both cases. The source of the irreversible component is suggested to be the loss of protein secondary structure through complexation between the ionic liquid components and the protein surface residues. The reversible electrochemical signal loss is likely due to interfacial interactions imposed between the electrode and the cytochrome heme group. The influence of the amount of exposed surface residues was explored with a simplified model protein, microperoxidase-11.
Published by Elsevier B.V.

Keywords: Cytochrome *c*; Ionic liquid; Cyclic voltammetry; Electrode immobilized protein; Self-assembled monolayer

1. Introduction

Non-aqueous biocatalytic systems have garnered much interest over the past decade because of their unique synthetic opportunities [1]. For example, hydrolytic enzymes (e.g. lipases and esterases) in non-polar, organic solvents with low water content have been shown to carry out reversed hydrolytic and transferase-type reactions. Recently, ionic liquids (ILs) have emerged as an alternative media to non-polar, hydrophobic solvents for supporting biocatalytic processes [2–6]. A myriad of organic cation and inorganic or organic anion combinations have allowed for these room temperature molten salts to be structured with convenient chemical and physical properties. ILs possess negligible vapor pressure, nonflammability, chemical and thermal stability, high ionic conductivity, and excellent electrochemical stability [7,8]. It should be noted that the toxicological and pharmacological effects of most ILs have yet to be delineated. With thoughtful selection of cationic and anionic components, ILs represent a neoteric, non-aqueous, polar class of solvents suitable for the development of 'green' biocatalytic processes [9].

The intrinsic conductivity and electrochemical stability of ILs make them an especially attractive non-aqueous media in which to study bioelectrocatalytic systems [8,10]. To date, relatively little data exist on the enzymatic activity of oxidoreductaces (e.g. desaturases, oxidases, and peroxidases) in ILs [11–13]. Recent studies have shown that the classic redox-active hemoprotein, cytochrome *c* (cyt-*c*), and analogues of its active site, microperoxidase-11 (MP-11) and protoporphyrin(IX) iron(III) chloride (hemin), condi-

☆ Product names are necessary to report factually on available data; however, the USDA neither guarantees nor warrants the standard of the product, and the use of the name by the USDA implies no approval of the product to the exclusion of others that may be suitable.

* Corresponding author. Tel.: +1 309 681 6324; fax: +1 309 681 6524.
E-mail address: comptond@ncaur.usda.gov (D.L. Compton).

1567-5394/$ - see front matter. Published by Elsevier B.V.
doi:10.1016/j.bioelechem.2005.01.002

tionally retain peroxidase activity in the ILs, 1-butyl-3-methylimidazolium bis(trifluoromethylsulfonyl)imide ([bmim][tf_2N]) and the hexafluorophosphate salts of 1-butyl- and 1-octyl-3-methylimidazolium ([bmim][PF_6] and [omim][PF_6], respectively) [14]. Cyt-*c* and its analogue MP-11 must be coordinated with a multi-dentate ligand [i.e. 2-(hydroxymethyl)-18-crown-6 ether] to retain peroxidase activity in the ILs. The lariat ether is necessary to solubilize the protein and is presumed to help maintain the non-supported enzyme's active conformation in polar, non-aqueous solvents [15].

To further investigate the potential use of redox active proteins and enzymes for bioelectrocatalytic synthesis in ILs we examined the electrochemical response of immobilized cyt-*c* as a model enzyme system. Cyt-*c* modified electrodes can be used to directly examine the protein's redox activity in ILs. Initial studies determined that the Fe(II)/Fe(III) redox couple of hemin-modified electrodes was stable in [alkylimidazolium][PF_6] salts without the need for additional electrolyte [16]. Similar studies were performed on cyt-*c* immobilized to mixed self-assembled monolayers (SAMs) of 11-mercaptoundecanoic acid (11-MUA) and 11-mercapto-1-undecanol (11-MU) supported on gold electrodes [17]. The redox activity of the immobilized cyt-*c* was lost upon prolonged exposure to neat [bmim][tf_2N] and [bmim][PF_6]. The cyt-*c* redox activity was reconstituted, however, when the electrodes were subsequently exposed to aqueous buffer. Polar organic solvents generally result in the loss of enzyme function, presumably due to the stripping of essential water from the enzyme [18]. This rationalization, however, is inadequate since water-saturated [bmim][tf_2N] (1.4% w/w) also did not support the redox activity of the immobilized cyt-*c* [17]. Thus, other confounding effects must contribute to the deleterious impact ILs have on the redox activity of the immobilized cyt-*c*.

The present work uses electrochemical, absorbance, and fluorescence methods to examine the specific effects of the aqueous solubilized IL components, $[bmim]^+$, 1-hexyl-3-methylimidazolium $[hmim]^+$, $[omim]^+$, $[tf_2N]^-$, $[PF_6]^-$, $[BF_4]^-$, and $[PO_4]^{3-}$ on the electron transfer response of cyt-*c* covalently bound to 1:1 mixed 11-MU/11-MUA SAMs supported on gold electrodes.

2. Experimental

2.1. Materials

Horse heart cyt-*c* prepared without trichloroacetic acid was purchased from Sigma-Aldrich and stored at −4 °C. Cyt-*c* purified via ion-exchange chromatography [19] was found to have identical behavior compared to the unpurified protein. Cyt-*c* was therefore used as received and without further purification for all experiments in this study. Microperoxidase-11 (MP-11), 11-mercaptoundecanoic acid (11-MUA), 11-mercapto-1- undecanol (11-MU), 1-[3(dimethylamino)propyl]3-ethylcarbodiimide hydrochloride (EDC), *N*-hydroxysuccinimide (NHS), 3-mercatopropanoic acid (3-MPA), 3-mercapto-1- propanol (3-MP) and reagent grade ethanol were also obtained from Sigma-Aldrich and used as received. ILs were obtained from ACROS Organics and stored in a dry nitrogen atmosphere chamber prior to use. Potassium phosphate buffer solutions (P_i) were prepared by using a mixture of potassium hydrogen phosphate and potassium dihydrogen phosphate with a combined total phosphate concentration of 10 mM. A pH of 7.0 was achieved by using a ratio between the two salts and confirmed by electronic pH measurement. Sodium chloride, ammonium chloride, and potassium nitrate were obtained from Fisher Scientific. Deionized water for this study was obtained using a Barnstead NANOpure Diamond model D11911 water purification system.

2.2. Electrode preparation

High purity gold wire (99.9998% pure) with a diameter of 0.5 mm was formed into a coil with a surface area of between 2.0 and 2.4 cm^2 either by Bioanalytical Systems (BAS) of West Lafayette, IN, or in house. Electrodes were cleaned initially and before each modification scheme using chemical and electrochemical polishing. Chemical polishing was composed of swirling the electrode in piranha solution (a 3:1 mixture between concentrated H_2SO_4 and 30% H_2O_2) for 60 s followed by a 15 min ultrasonic rinse in D.I. H_2O. After three repetitions of chemical polishing, the electrode was subjected to an electrochemical polish step. Electrochemical polishing was accomplished by using the gold coil electrode as the working electrode (WE) in a three electrode cell in combination with a platinum wire counter electrode (CE) and a $Ag/AgCl/NaCl_{(3M)}$ reference electrode (RE, E vs. SHE = 206 mV). The working electrode was subjected to a 50 cycle potential sweep between 1.50 V and −0.30 V in 1.0 M H_2SO_4, after which the characteristic cyclic voltammogram for this system was obtained [20]. The electrode surface roughness was determined by integrating the charge under the gold oxide reduction peak in the sulfuric acid voltammograms. A value of 482 μC cm^{-2} for monolayer coverage of oxygen on a gold electrode was equated to a surface roughness of 1.0 [21].

After polishing, the electrodes were immediately coated with a mixed SAM of 11-MU and 11-MUA. Coating was accomplished by incubating the electrode for 24 h in a solution composed of 5 mM 11-MU and 5 mM 11-MUA dissolved in ethanol. Electrodes were rinsed with ethanol and a solution of 10% acetic acid in ethanol after removal from the SAM bath. This step was included to remove electrostatically bound 11-MU and 11- MUA from the electrode surface [22].

Covalent attachment of cyt-*c* was accomplished by first activating the SAM surface by placing the modified electrode into an aqueous solution of 200 mM EDC and 50 mM NHS for 10 min. The activated electrode was then

rinsed with buffer and placed into a 50 μM cyt-*c* solution for 3 h. Electrostatically adsorbed cyt-*c* was removed by rinsing the electrode with aqueous 10% acetic acid, followed by D.I. H_2O immediately prior to use.

2.3. Cyclic voltammetry (CV)

Voltammograms were obtained using a BAS CV-50W voltammetric analyzer in combination with a BAS C3 cell stand. A standard three electrode configuration was used for all experiments. This configuration utilized a platinum wire CE, a Ag/AgCl/$NaCl_{(3M)}$ RE, and the modified gold coil as the WE. Solutions were purged of oxygen by bubbling dry nitrogen through the cell solution before experiments and a nitrogen atmosphere was maintained over the solution during measurement of voltammograms. CV data were recorded with a scan rate of 50 mV/s. The pH 7.0 reduction potential ($E^{\circ\prime}$) was calculated as the midpoint between the oxidation and reduction peaks and listed as relative to the RE potential (E = 0.206 V vs. SHE) unless otherwise noted.

2.4. Peroxidase assay

Electrode-immobilized MP-11 was examined for peroxidase activity by following the oxidation of 1.0 mM 2,2′-azino-bis(3-ethylbenzthiazoline-6-sulfonate) (ABTS) optically at 416 nm with a Shimadzu 1240 spectrophotometer equipped with a kinetics module. A cuvette (1 × 1 cm) was charged with 2.5 mL of 10 mM P_i, pH 7.0, containing 1.0 mM ABTS and 1.0 mM H_2O_2. Following immobilization on the SAM (11-MU/11-MUA) modified surface, the electrode was rinsed extensively with water to remove adhering solution phase MP-11. The electrode was then transferred to the cuvette, agitated by hand, and then briefly withdrawn at 60 s intervals.

2.5. Fluorescence measurements

Fluorescence measurements were obtained on a Varian Cary-Eclipse fluorometer where the samples were temperature-controlled in a four-position Peltier cuvette holder. Temperature was maintained at 23 ± 0.03 °C. Emission spectra were measured with an excitation of 295 nm and slits (excitation/emission) at 10 nm each. Cyt-*c* was added at 10 μM to [bmim]Cl or Li[tf_2N] at various concentrations. Reported spectra were the result of averaging the individual spectra of three or four samples, each sample having been scanned three to six times to ensure spectral stability.

3. Results and discussion

3.1. Immobilization of cyt-c

When CV was performed on cyt-*c* modified electrodes in P_i buffer, a reversible current signal was observed for a redox process with an $E^{\circ\prime}$ of −42 ± 7 mV and a peak separation of 34 ± 3 mV (n = 10 electrodes). This signal is consistent with the Fe(II)/Fe(III) redox process of covalently immobilized cyt-*c* on a MU/MUA electrode as reported by Lisdat [23] as well as previously measured by Compton and Laszlo [17]. This signal was stable for more than ten successive cycles and for greater than 120 min in pH 7.0 P_i buffer. Through integration of the background subtracted reduction peak and the assumption of a one electron process, the cyt-*c* surface coverage was calculated to be 4.0 ± 0.5 pmol/cm^2. This value is consistent with the surface coverage previously measured by Compton and Laszlo [17] and approximately half of the coverage reported by Lisdat using a similar electrode modification scheme [23].

To confirm that the cyt-*c* was covalently immobilized to the MU/MUA modified gold, the electrodes were exposed to high ionic strength aqueous solutions. The cyt-*c* redox signal was observed in up to 1.0 M NaCl, LiCl, KNO_3, and NH_4Cl aqueous solutions without the loss of current signal. Electrostatically bound cyt-*c* typically desorbs from the MU/MUA surface at these molar salt concentrations resulting in the loss of redox signal [24]. Thus, the covalent immobilization of the cyt-*c* was successful.

A positive shift in the covalently immobilized cyt-*c* reduction potential was observed with increasing ionic strength and is similar to previous findings by Clark and Bowden where a positive shift in $E^{\circ\prime}$ was reported for cyt-*c* electrostatically immobilized on an 11-MUA SAM in increasing ionic strength solution [24]. Gavioli et al. have also reported a positive shift of reduction potential with increasing ionic strength for cyt-*c* electrostatically immobilized on an 11-MU SAM [25].

A similar positive shift of the covalently immobilized cyt-*c* redox potential was also observed upon exposure to the IL components (Fig. 1). The deleterious effects that the IL components have on the cyt-*c* current signal discussed below, however, cannot be attributed to simple ionic strength effects. Furthermore, these adverse effects on the cyt-*c* current cannot be attributed to the influence of the IL component counter ions (Li^+, Na^+, K^+, NH_4^+, and Cl^-) or the desorption of the cyt-*c* from the electrode surface.

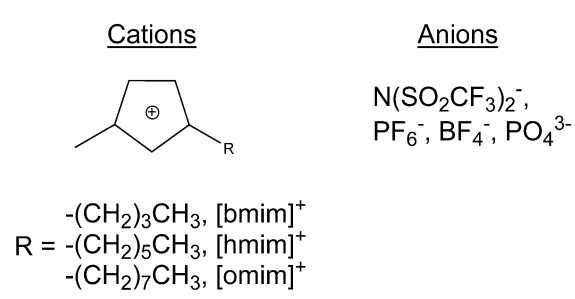

Fig. 1. Ionic liquid cationic and anionic components.

3.2. Ionic liquid cation exposure

In the presence of [bmim]Cl, a shift in the cyt-*c* $E^{\circ\prime}$ to more positive potentials was observed (Fig. 2). This effect can be explained by the increase in ionic strength of the solution, similar to the potential shift seen in NaCl, LiCl, KNO_3, and NH_4Cl solutions discussed above. Although the IL cation component is organic in nature, the redox potential of the cyt-*c* does not become more negative as observed when the protein is exposed to other water-miscible organic solvents such as dimethyl sulfoxide, dimethylformamide, and acetonitrile. These organic solvents lower the dielectric of the aqueous solution, resulting in alkaline-like misligated states of the cyt-*c* [26]. The IL components studied herein, however, dissociate as ions in water, effectively raising the dielectric of the media. Thus, a positive shift of the cyt-*c* redox potential is not unexpected and has been previously observed [24,25].

Contrary to the unchanged current response observed with increasing concentration of NaCl, increasing concentrations of [bmim]Cl resulted in a progressive decrease in the cyt-*c* current signal (Fig. 2). The loss of the cyt-*c* current signal was independent of the scan rate from 50 to 500 mV/s. At 1.0 M [bmim]Cl, the electrochemical signal was not entirely suppressed as it was in neat [bmim][PF_6] and [bmim][tf_2N] [16]. After a series of [bmim]Cl solution treatments (up to 1.0 M), ~65% of the cyt-*c* redox signal returned when the electrode was rinsed well and placed into fresh P_i buffer. This recovered redox signal occurred at an $E^{\circ\prime}$ value that was negatively shifted ~15 mV in comparison to the unexposed cyt-*c* signal. Recovery of the redox signal confirms that cyt-*c* is not removed from the electrode surface upon exposure to [bmim]Cl. The lesser current and negative shift in $E^{\circ\prime}$ in the recovered signal indicates that, in addition to a reversible signal loss, an irreversible process is also occurring.

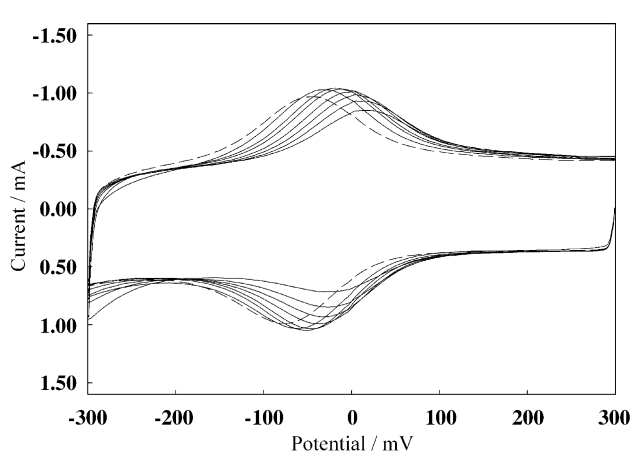

Fig. 2. Typical CVs of immobilized cyt-*c* on a gold electrode in phosphate buffer (pH 7) exposed to progressively higher concentrations of [bmim]Cl (—). Signal decreases with higher concentration of [bmim]Cl. CV of the same electrode rinsed and reconstituted in fresh phosphate buffer (---).

Loss of the cyt-*c* current signal in [bmim]Cl solution may be caused by one or more different effects such as a structural change within the heme ligation state that suppresses the Fe(II)/Fe(III) redox couple, an interruption of the electron transfer pathway between the electrode and the cyt-*c* heme, or an increase in electrode to heme distance.

The loss of the cyt-*c* signal is not likely caused by a direct interaction of the $[bmim]^+$ with the heme iron, resulting in a change of the heme ligation state. The dialkyl imidazolium cation (Fig. 1) lacks a free nitrogen electron lone pair found in such bases as *N*-methyl imidazol and pyridine. These nitrogenous coordinating bases shift the redox potential of cyt-*c* heme center more negative [16]. Exposure of immobilized cyt-*c* to $[bmim]^+$ results in a positive shift in its redox potential (Fig. 2). The loss of the cyt-*c* redox signal when exposed to $[bmim]^+$ would more likely be due to the cation's influence on the protein's secondary structure. Changes in the extended protein structure have been shown to have a strong impact on the thermodynamics of redox couples [27]. If the redox thermodynamics shift to unfavorable conditions through unfolding or denaturation of the protein then loss of the cyt-*c* current signal within the potential window of our experiments would be observed. The possible influence of $[bmim]^+$ on the cyt-*c* secondary structure is explored using absorbance and fluorescence spectroscopy, discussed below.

As $[bmim]^+$ contains a significant non-polar organic region (Fig. 1) one must consider the possibility that the cation's tail may likely partition into the hydrophobic environment of the SAM. This accumulation of the $[bmim]^+$ in the SAM layer could possibly lessen the cyt-*c* redox signal by increasing the organic density between the electrode and the protein, which would most likely lessen the electron's ability to tunnel to the protein. To examine this possibility, two additional IL cations were used with longer hydrophobic chain lengths, [hmim]Cl and [omim]Cl, where the butyl alkyl chain is replaced by a hexyl and octyl group respectively. The increased hydrophobic nature of the $[hmim]^+$ and $[omim]^+$ as compared to $[bmim]^+$ would be expected to increase the level of partitioning into the highly hydrophobic inner regions of the SAM layer. A greater signal loss at lower concentrations would then be expected with the longer chain length species as they more significantly partition into the SAM, insulating against the electrode–protein electron-transfer.

Both of the longer chain length cations were found to result in a greater loss of the cyt-*c* current signal as shown in Fig. 3. Because the initial coverage of cyt-*c* varied somewhat between electrodes, the experiments were normalized by reporting the redox active surface coverage as the percentage of the initial redox active coverage remaining after exposure to an increasing concentration of IL. The $[omim]^+$ ion might be expected to partition more greatly than $[hmim]^+$ into the SAM due to its greater hydrophobic surface area, yet $[omim]^+$ resulted in less of a deleterious effect on the cyt-*c* redox signal (Fig. 3). A possible

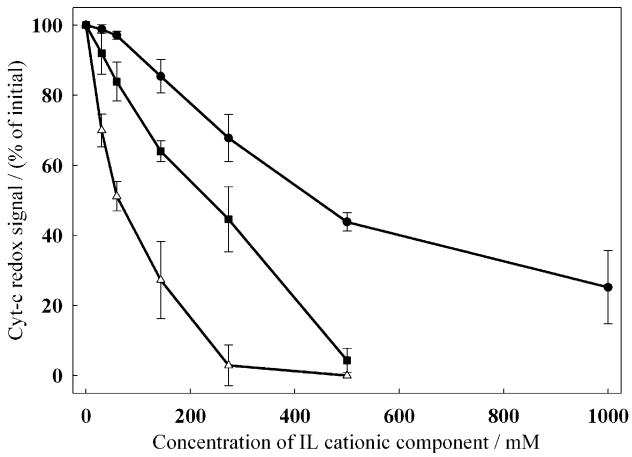

Fig. 3. Influence of (●) [bmim]Cl, (Δ) [hmim]Cl, and (■) [omim]Cl on immobilized cyt-*c* redox current. Error bars represent one standard deviation ($n=4$).

explanation for the lesser effect of $[omim]^+$ is from steric hindrance arising from a non-uniform density of the SAM layer. Similar to the straws in the head of a broom where the point of attachment is denser than the unattached outer edge, the density of the SAM molecules may be more diffuse at the solution–SAM boundary than at the electrode interface. This increasing density at greater SAM depth could sterically hinder molecules partitioning into the layer after a maximum chain length is reached. Overall, both the longer chain length IL cations caused greater loss of the cyt-*c* redox current than the $[bmim]^+$. These data support the possibility that the IL cations may intercalate into the SAM, and that the intercalation is dependent on the IL cation alkyl chain length.

If any intercalation of the IL cations into the SAM occurs, it appears to be reversible, as a significant portion of the cyt-*c* signal returns after rinsing the electrode with 10 mM P_i buffer. As complete reversibility is not achieved, the question of the nature of the unrestored portion of the CV signal naturally arises. To examine the effect of the IL cations on the SAM, electrodes were coated with 11-MU/11-MUA and then incubated for 30 min in 200 mM solutions of [bmim]Cl, [hmim]Cl, or [omim]Cl. The IL-treated electrodes were then rinsed with 10% acetic acid and D.I. H_2O to remove any electrostatically adsorbed species before covalent attachment of cyt-*c* was performed. No difference in cyt-*c* signal compared to untreated electrodes was observed, indicating that the exposure of the SAM to the IL cations did not result in irreversible alteration of the alkylthiol monolayer. Electrochemical impedance spectroscopy measurements of the 11-MU/11-MUA SAM layer before and after exposure to the three IL cationic components confirmed these findings. The impedance of the SAM did not change after exposure to 1.0 M solutions of the three cations for 72 h followed by rinsing and immersion in P_i buffer. Additionally, blocking studies using $K_3Fe(CN)_6$ as a redox probe showed no current signal by CV for 11-MU/11-MUA SAM modified gold electrodes before and during exposure to [bmim]Cl, suggesting that the $[bmim]^+$ does not disrupt the SAM. These results suggest that the unrecoverable loss of the immobilized cyt-*c* redox signal upon exposure to [bmim]Cl cannot be attributed to an irreversible interaction of the $[bmim]^+$ with the 11-MU/11-MUA SAM. The possibility that the partial, unrecoverable loss of redox signal results from some irreversible change in cyt-*c* structure resulting from interactions with the IL cation is examined further in the spectroscopy section (vide infra).

A third possibility for the loss of the cyt-*c* redox signal when exposed to the IL cations is an increase in electron donor–receptor distance. An increase in electrode–protein distance has generally been described to result in an exponential decrease in the electron transfer rate [28]. The loss of the redox signal of cyt-*c* due to increased distance between the heme and the electrode would imply that the distance has increased to where the electron transfer becomes less favorable to the extent that it is not observed at the scan rates used in this study.

Although cyt-*c* is covalently anchored to the electrode surface through one or more lysine residues for the present study, including most likely Lys13 [29], many lysine residues exist on the protein surface that may be required for maintaining a functional orientation and electrode–heme distance through electrostatic interactions. Niki et al. [30] have shown that the electron transfer rate can decrease by over an order of magnitude for proteins on a carboxyl terminated alkylthiol SAM with each additional CH_2 group beyond a 10 carbon chain length. Disruption of the lysine–surface interactions, outside of the covalent anchor, by the $[bmim]^+$ cation may cause reorientation of the protein that could increase the heme-electrode distance.

Due to the complexity of the possible effects caused by the cationic IL components, absorption and fluorescence spectroscopy, as well as comparison to MP-11, were used to better elucidate the mechanism of the cyt-*c* redox signal loss.

3.3. Ionic liquid anion exposure

In addition to cationic IL components, the anionic component $[tf_2N]^-$ was examined by using the lithium salt, $Li[tf_2N]$. Like the cationic IL components, $Li[tf_2N]$ produced a loss of cyt-*c* signal (Fig. 4), which was not observed in the presence of the simpler Cl^- anion. This loss occurred to a degree similar to that of the $[hmim]^+$ and $[omim]^+$ and more than that of $[bmim]^+$. As $[tf_2N]^-$ is a much more polar molecule than the [imidazolium] cations, incorporation into the SAM layer would not be expected to occur to an appreciable extent.

The influence of two other common IL anions on the cyt-*c* redox signal was examined. The ammonium salts of $[BF_4]^-$ and $[PF_6]^-$ produced a loss of cyt-*c* signal with increasing concentration (Fig. 4). The $[PF_6]^-$ was more deleterious to the cyt-*c* redox signal than $[BF_4]^-$. The loss

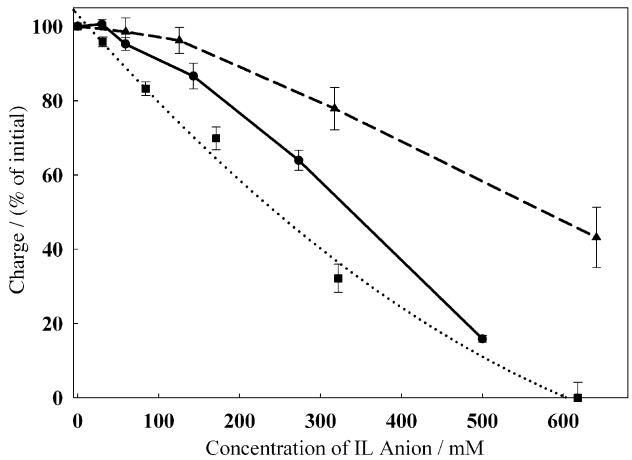

Fig. 4. Influence of (●) Li[tf_2N], (▲) [NH_4][BF_4], and (■) [NH_4][PF_6] on immobilized cyt-*c* redox current. Error bars represent one standard deviation (n=4).

of cyt-*c* signal in the presence of the poorly coordinating [tf_2N]$^-$ anion was greater than that due to the [BF_4]$^-$, and less than the loss due to the [PF_6]$^-$.

[PO_4]$^{3-}$ proved to be the harshest anion on the cyt-*c* redox signal, resulting in the complete loss of signal at a concentration of 27 mM (data not shown). The pH of the 27 mM [PO_4]$^{3-}$ solutions were >10. The alkaline environment is presumed to have caused the conformational rearrangement to a mixture of misligated states. These conformational changes most likely render the immobilized cyt-*c* redox inactive.

The pH of the [tf_2N]$^-$, [BF_4]$^-$, [PF_6]$^-$ solutions (>500 mM) was found to be ~7, therefore, the cyt-*c* was not subjected to the same alkali-induced conformational changes in these solutions. These complex anions, however, must interact with the immobilized protein in some way which renders it redox inactive. These anion–protein interactions were investigated using absorbance and emission spectroscopy.

3.4. Absorbance spectroscopy

Loss of the cyt-*c* 695 nm visible absorption band at room temperature indicates a disruption of the coordination of the native Met80 heme ligand, such as that seen with the acid-unfolded pH 2.7 form of the protein [31]. The position and intensity of the Soret band are also indicative of the integrity of the heme pocket. P_i buffer (pH 7.0) solutions of cyt-*c* containing up to 1.0 M NaCl showed a modest increase in the intensity at 695 nm and no change in the Soret band position compared to cyt-*c* freshly reconstituted in P_i buffer from the lyophilized state (Table 1). The increased intensity of the 695-nm charge-transfer band may result from closer heme–Met80 interactions. In contrast, [bmim]Cl added above 0.2 M led to an increasing loss of the 695-nm band, with about 52% retention of Met80 ligation at 1.0 M. There was no significant change in the position of the Soret absorption maximum with NaCl or [bmim]Cl, indicating that the heme environment remained otherwise intact with either salt. The progressive loss of the Met80 ligation at higher [bmim]$^+$ concentrations corresponds to the progressive loss of the immobilized cyt-*c* redox signal. If the initial loss of the cyt-*c* redox current observed below 200 mM [bmim]$^+$ (Fig. 3) results from a protein–[bmim]$^+$ interaction, this interaction does not perturb the heme pocket. Perturbation of the heme pocket was only observed at higher [bmim]$^+$ concentrations (>500 mM; Table 1).

[Bmim]Cl treatment of immobilized cyt-*c* results in a loss of redox activity that is only partially recovered with removal of the IL. As discussed above, this irretrievable portion of the cyt-*c* redox activity could not be attributed to changes in the SAM layer. As an alternative possibility, permanent changes in the cyt-*c* structure may have been induced by the IL. This possibility was examined by treating cyt-*c* with either 1.0 M NaCl or 1.0 M [bmim]Cl, followed by exhaustive dialysis (5 d) of the protein against P_i buffer. The NaCl-treated cyt-*c* fully retained its enhanced 695-nm absorbance (120% compared to buffer-alone solubilized cyt-*c*) after dialysis. This suggests that 1.0 M NaCl induces a permanent change in the heme cavity, i.e., greater heme–Met80 interaction. Dialysis of [bmim]Cl-treated cyt-*c* dramatically reversed the loss of the charge-transfer interactions in the heme cavity to the extent that the 695-nm band intensity increased to 137% of that of the control, untreated cyt-*c*. Thus [bmim]Cl-induced heme ligation changes appear to be fully reversible, resulting in a state comparable to that induced by NaCl treatment. Recalling that 1.0 M NaCl did not alter the redox signal intensity of the immobilized cyt-*c*, the [bmim]Cl-induced irretrievable cyt-*c* redox activity is not attributable to changes in heme ligation, nor any heme cavity change detectable by absorption spectroscopy. Differences between the NaCl- and [bmim]Cl-treated, dialyzed, cyt-*c* observed by fluorescence spectroscopy are described below.

Table 1
Changes in cyt-*c* absorbance spectrum due to [bmim]Cl and Li[tf2N]

Salt conditions[a]	695 nm absorption intensity[b]/(%)	Soret band position[c]/nm
10 mM buffer	100	409
0.2 M NaCl	121	409
0.5 M NaCl	121	409
1.0 M NaCl	124	409
0.2 M [bmim]Cl	103	408
0.5 M [bmim]Cl	86	408
1.0 M [bmim]Cl	52	408
0.2 M Li[tf_2N]	5	405
18 mM HCl	0	394

[a] All solutions, except 18 mM HCl, contained 10 mM phosphate buffer, pH 7.0.
[b] Relative absorption of 250 μM cyt-*c* in the indicated salt solution, less the absorption of acid unfolded cyt-*c*: (Salt695 nm − HCl695 nm)/(Phosphate695 nm − HCl695 nm).
[c] Cyt-*c* concentration 5 μM.

The effect of $[tf_2N]^-$ on the cyt-*c* absorbance spectrum was much more pronounced than that of $[bmim]^+$. $Li[tf_2N]$ (0.2 M) effectively eliminated Met80 ligation in the heme pocket and was accompanied by a 3 nm blue shift in the Soret absorption band. Concentrations of 0.5 M $Li[tf_2N]$ and above resulted in protein aggregation and precipitation. Thus, $[tf_2N]^-$ is assumed to be far more disruptive than $[bmim]^+$ on the structure of cyt-*c* in aqueous media. A far more disruptive influence of $[tf_2N]^-$ compared to $[bmim]^+$ is not observed in the electrochemical measurements. Instead, the loss of the cyt-*c* redox signal observed in the presence of 0.2 M $[tf_2N]^-$ is only ~5% greater than in the presence of 0.2 M $[bmim]^+$. It is likely that the immobilization of the cyt-*c* on the alkylthiol SAM stabilizes the protein, lessening the $[tf_2N]^-$ ability to disrupt the protein's secondary and tertiary structure.

3.5. Fluorescence spectroscopy

Fluorescence emission has been used to follow structural changes induced by the aqueous environment of cyt-*c* [32–34]. With excitation at 295 nm, emission from the tryptophan of cyt-*c* is seen at 348 nm. Within the folded native cyt-*c* environment the tryptophan fluorescence is strongly quenched by the heme-group as well as nearby amino acids. When protein unfolding occurs, the distance between the tryptophan and the heme increases. This increased distance reduces the level of quenching and results in greatly increased tryptophan fluorescence, which can be monitored directly as an indication of the loss of secondary structure in cyt-*c* [35]. Fig. 5 shows the fluorescence spectra of 10 μM cyt-*c* in its native (pH 7.4) and acid denatured (pH 2.7) states.

Addition of 5 mM [bmim]Cl to a 10 μM cyt-*c* solution (pH 7.4) greatly influenced the emission spectrum (Fig. 6). The single 348 nm peak associated with the tryptophan fluorescence was replaced by two new peaks. The first of these peaks was red-shifted from the tryptophan peak to 369 nm and the second peak occurs near 432 nm. In addition, the emission peak at 416 nm observed in both the 5.0 (and 500, not shown) mM [bmim]Cl blank was quenched in the presence of cyt-*c*. This change in the $[bmim]^+$ emission spectrum may suggests that the cyt-*c* interacts with the $[bmim]^+$, forming a complex with a unique emission spectrum. However, the cyt-*c* Soret band occurs at 409 nm. Thus, it is possible that the two peaks (369 nm and 432 nm) are actually the $[bmim]^+$ emission peak with the loss of intensity at 409 nm due to absorbance by cyt-*c*. Therefore, the emission data of $[bmim]^+$ in the presence of cyt-*c* (Fig. 6) do not provide definitive evidence of a $[bmim]^+$–cyt-*c* interaction. The emission data cannot be used to clarify the influence of the $[bmim]^+$ on the cyt-*c* that was observed by CV and absorbance experiments.

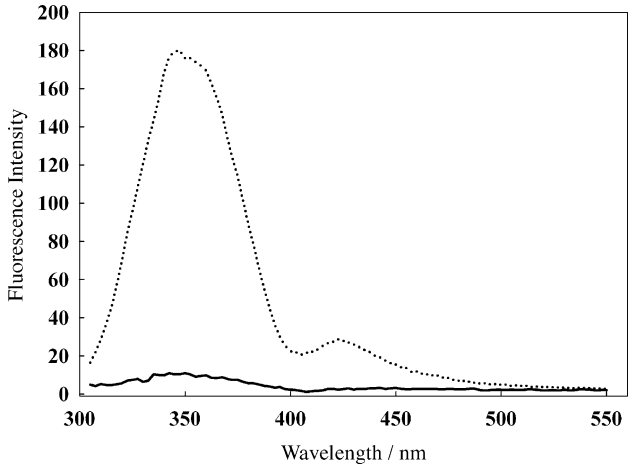

Fig. 5. Emission spectra of cyt-*c* in (—) pH 7.4 and (· · ·) pH 2.7 solutions.

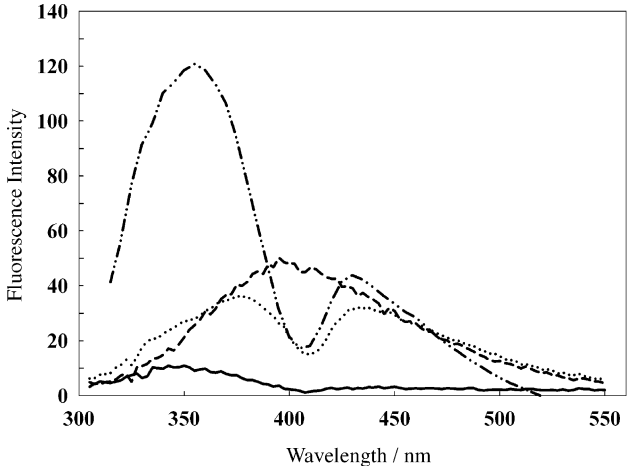

Fig. 6. Emission spectra of (—) cyt-*c*, (---) [bmim]Cl, and the possible cyt-*c*/[bmim]Cl complex at (· · ·) pH 7.4 and (-●●-) pH 2.7.

While the change in the $[bmim]^+$ spectrum did not provide conclusive evidence of a $[bmim]^+$ and cyt-*c* interaction, it was clear that the more intense $[bmim]^+$ signal overwhelmed the cyt-*c* spectrum. This may have masked any changes in the cyt-*c* spectrum. Therefore, the emission spectrum of untreated cyt-*c* was compared to cyt-*c* that had been exposed to [bmim]Cl that was subsequently removed by dialysis. Cyt-*c* treated with 1.0 M [bmim]Cl and then dialyzed displayed a slight blue shift in the fluorescence spectrum (data not shown), indicating greater incorporation into the non-polar environment of the heme cavity [36]. This shift was not observed when the experiment was conducted with 1.0 M NaCl. This suggests that $[bmim]^+$ either remains very tightly bound to cyt-*c* after extensive dialysis, or [bmim]Cl-induced changes in cyt-*c* secondary structure are retained after removal of the IL. This retained structural influence of [bmim]Cl may be responsible for the observed partial, unrecoverable loss of redox signal noted with immobilized cyt-*c*.

The emission spectrum of cyt-*c* in the presence of $Li[tf_2N]$ showed that the $[tf_2N]^-$ had a minor influence on cyt-*c* at moderate concentrations, 30 to 273 mM (Fig. 7). The slightly less quenched tryptophan peak (348 nm) at 273

mM Li[tf_2N] shows that the protein structure is only slightly changed. This is counter to what was observed in the absorbance assay where the cyt-*c* experiences complete loss of the Met80 ligation to the heme iron (Table 1). Therefore, $[tf_2N]^-$ must more directly affect the cyt-*c* heme pocket than the protein tertiary structure at moderate concentrations. This, however, results in only a slightly increased loss of cyt-*c* redox current when compared to the influence of the $[bmim]^+$ at similar concentrations (273 mM). At higher $[tf_2N]^-$ concentrations (500 mM) the emission spectrum indicates that the cyt-*c* is completely denatured. This is consistent with the nearly complete loss of cyt-*c* redox signal observed at similar $[tf_2N]^-$ concentrations (Fig. 4).

3.6. Microperoxidase-11

In order to examine a more simplified system, MP-11/SAM modified electrodes were also constructed. MP-11 consists of an iron-containing heme moiety in conjunction with an eleven amino acid secondary structure. MP-11 therefore acts as a model of the heme pocket with a minimum of additional protein scaffolding. This simplification allows for further elucidation of IL component interactions with the cyt-*c* protein scaffolding.

CV did not show a redox process within a −400–+600 mV potential window for MP-11 on 11-MU/11-MUA electrodes, but the presence and continued enzyme activity of MP-11 on the electrode was confirmed through a colorometric microperoxidase activity assay (Fig. 8). A catalytic wave was also detected using the MP-11 modified electrode in the presence of 30 mM H_2O_2. The bare SAM surface did not display a catalytic wave CV when exposed to H_2O_2. Catalytic current signals can be observed in CV when both an enzyme and an appropriate substrate for that enzyme are present. The presence of a catalytic wave when attempted immobilization of MP-11 had been performed, along with the absence of the wave from bare SAM electrodes, is additional evidence that MP-11 was successfully immobilized on the electrode surface. Although the MP-11 was successfully immobilized on the 11-MU/11-MUA SAM and exhibited catalytic activity, the Fe(II)/Fe(III) redox couple was not observed by CV.

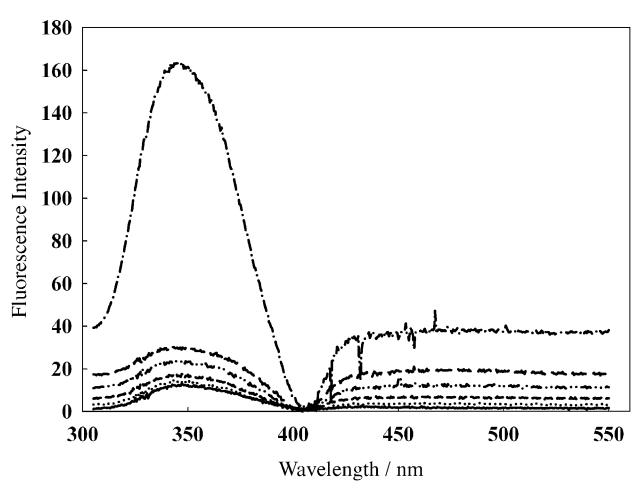

Fig. 7. Emission spectra of cyt-*c* in (—) 0, (· · ·) 30, (---) 59, (-●●-) 143, (–·–) 273, and (-●-) 500 mM Li[tf_2N] concentration. Signal strength increases with increasing concentration of Li[tf_2N].

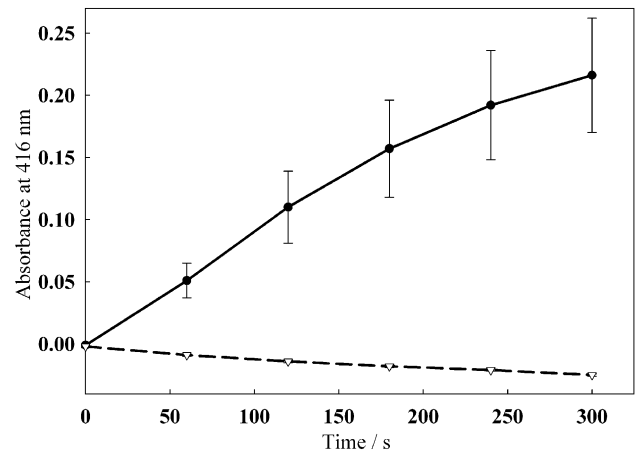

Fig. 8. Kinetic results of colorimetric peroxidase assay on MP-11. (●) MP-11:SAM modified electrode, (Δ) SAM modified electrode.

4. Conclusions

The loss of Fe(II)/Fe(III) redox activity of cyt-*c* covalently attached to 11-MU/11-MUA modified electrodes in the presence of the neat ionic liquid [bmim][tf_2N] was found to also occur when the electrodes were exposed to the cationic and anionic components separately. The mechanism by which the redox activity is lost differs, however, in the two cases. Our results suggest that the alkylimidazolium cations may intercalate into the SAM layer causing a disruption of the attachment site leading to non-ideal distance and orientation of the heme center. When the cyt-*c* modified electrode is exposed to the longer chain alkylimidazolium cations the loss of cyt-*c* redox signal, as measured by CV, occurs at a lower concentration of salt (Fig. 3). This indicates that partitioning of the cation into the monolayer may be occurring and that the increased hydrophobicity of the longer chain IL cation leads to greater partitioning and, therefore, a greater extent of redox signal loss. Absorbance spectroscopy shows that the local heme environment of solutionary cyt-*c*, as evidenced by the Met80–heme ligation, is only affected at concentrations of $[bmim]^+$ over 0.5 M and that the heme cavity structure, as monitored by the Soret band, is unchanged even at 1.0 M $[bmim]^+$ (Table 1). This suggests that the loss of cyt-*c* redox signal in the presence of $[bmim]^+$ is due to a disruption of the electron transfer at the SAM/enzyme interface rather than denaturation of the cyt-*c*.

In contrast, $[tf_2N]^-$ was found to directly cause protein unfolding. Absorbance spectra indicated that Met80 ligation

is lost at concentrations of $[tf_2N]^-$ below 200 mM, as evidenced by the loss of the 695 nm band (Table 1) although the lack of a large shift in the Soret band (409 nm vs. 408 nm in the native cyt-*c*) shows that only partial unfolding of the protein secondary structure has occurred at this concentration. Emission results also support an interpretation of a partial loss of structural integrity as the spectrum of the $[tf_2N]^-$ exposed cyt-*c* shows only minor changes in tryptophan intensity up to 200 mM $[tf_2N]^-$ concentration (Fig. 7), although complete loss of secondary structure is indicated by the large change in the emission spectrum at concentrations at or above 500 mM.

To prevent loss of the redox signal in ILs, the addition of protecting groups to the protein surface can be explored to determine if the secondary structure of the protein can be protected from interaction with the IL components. The addition of a protecting layer over the existing cyt-*c* modified electrode surface is a second option. Under this scheme, the secondary layer selected should be permeable to substrate, but exclude potentially damaging IL from reaching the enzyme or SAM. Finally, with the large number of existent and emerging ILs it may be possible to fine tune the physical characteristics of the cationic and anionic components to support the redox activity of immobilized cyt-*c*.

Acknowledgments

The authors thank Dr. Fred Lisdat for his helpful conversations and suggestions. The authors also thank Kendra B. Brandon and Leslie J. Smith for their excellent technical assistance, and Dr. David J. Sessa for the generous loan of his fluorometer.

References

[1] G.R. Castro, T. Knubovets, Homogeneous biocatalysis in organic solvents and water–organic mixtures, Crit. Rev. Biotechnol. 23 (2003) 195–231.
[2] R.A. Sheldon, R.M. Lau, M.J. Sorgedrager, F. van Rantwijk, K.R. Seddon, Biocatalysis in ionic liquids, Green Chem. 4 (2002) 147–151.
[3] R.A. Sheldon, Catalytic reactions in ionic liquids, Chem. Commun. (2001) 2399–2407.
[4] S. Park, R.J. Kazlauskas, Biocatalysis in ionic liquids—advantages beyond green technology, Curr. Opin. Biotechnol. 14 (2003) 432–437.
[5] F. van Rantwijk, R.M. Lau, R.A. Sheldon, Biocatalytic transformations in ionic liquids, Trends Biotechnol. 21 (2003) 131–138.
[6] U. Kragl, M. Eckstein, N. Kaftzik, Enzyme catalysis in ionic liquids, Curr. Opin. Biotechnol. 13 (2002) 565–571.
[7] H. Zhao, S.V. Malhotra, Applications of ionic liquids to organic synthesis, Aldrichimica Acta 3 (2002) 75–83.
[8] B.M. Quinn, Z. Ding, R. Moulton, A.J. Bard, Novel electrochemical studies of ionic liquids, Langmuir 18 (2002) 1734–1742.
[9] R.D. Rogers, K.R. Seddon (Eds.), Ionic Liquids: Industrial Applications to Green Chemistry, ACS Symposium Series 818, American Chemical Society Press, Washington, DC, 2002.
[10] P.A.Z. Suarez, V.M. Selbach, J.E.L. Dullius, S. Einloft, C.M.S. Piatnicki, D.S. Azambuja, R.F. de Souza, J. Dupont, Enlarged electrochemical window in dialkyl-imidazolium cation based room-temperature air and water-stable molten salts, Electrochim. Acta 42 (16) (1997) 2533–2535.
[11] G. Hinckley, V.V. Mozhaev, C. Budde, Y. Khmelnitsky, L, Oxidative enzymes possess catalytic activity in systems with ionic liquids, Biotechnol. Lett. 24 (2002) 2083–2087.
[12] K. Okrasa, E. Guibe-Jampel, M. Therisod, Ionic liquids as a new reaction medium for oxidase-peroxidase-catalyzed sulfoxidation, Tetrahedron: Asymmetry 14 (2003) 2487–2490.
[13] J. Howarth, P. James, J. Dai, Immobilized baker's yeast reduction of ketones in ionic liquid [bmim]PF_6 and water mix, Tetrahedron Lett. 42 (2001) 7517–7519.
[14] J.A. Laszlo, D.L. Compton, Comparison of peroxidase activities of hemin, cytochrome *c* and microperoxidase-11 in molecular solvents and imidazolium-based ionic liquids, J. Mol. Catal., B Enzym. 18 (2002) 109–120.
[15] T. Yamada, S. Shinoda, K. Kiwawa, A. Ichimura, J. Teraoka, T. Takui, H. Tsukube, Supramolecular complex of cytochrome *c* with lariat ether: solubilization, redox behavior and catalytic activity of cytochrome *c* in methanol, Inorg. Chem. 39 (2000) 3049–3056.
[16] D.L. Compton, J.A. Laszlo, Direct electrochemical reduction of hemin in imidazolium-based ionic liquids, J. Electroanal. Chem. 520 (2002) 71–78.
[17] D.L. Compton, J.A. Laszlo, Loss of cytochrome *c* Fe(III)/Fe(II) redox couple in ionic liquids, J. Electroanal. Chem. 553 (2003) 187–190.
[18] M.N. Gupta, Enzyme function in organic solvents, Eur. J. Biochem. 203 (1992) 25–32.
[19] S. Ye, C. Shen, T.M. Cotton, N.M. Kostic, Characterization of zinc-substituted cytochrome *c* by circular dichroism and resonance Raman spectroscopic methods, J. Inorg. Biochem. 65 (1997) 219–226.
[20] M. Peuckert, F.P. Coenen, H.P. Bonzel, On the surface oxidation of a gold electrode in H2SO4 electrolyte, Surf. Sci. 14 (1984) 515–532.
[21] U. Oesch, J. Janata, Electrochemical study of gold electrodes with anodic oxide films—I. Formation and reduction behavior of anodic oxides on gold, Electrochim. Acta 28 (1983) 1237–1246.
[22] L. Li, S. Chen, S. Jiang, Protein adsorption on alkanethiolate self-assembled monolayers: nanoscale surface structural and chemical effects, Langmuir 19 (2003) 2974–2982.
[23] F. Lisdat, B. Ge, Superoxide sensor based on cytochrome *c* immobilized on mixed-thiol SAM with a new calibration method, Anal. Chim. Acta 454 (2002) 53–64.
[24] R.A. Clark, E.F. Bowden, Voltammetric peak broadening for cytochrome *c*/alkanethiolate monolayer structures: dispersion of formal potentials, Langmuir 13 (1997) 559–595.
[25] G. Gavioli, M. Borsari, M. Cannio, A. Ranieri, G. Volponi, Redox thermodynamics of cytochrome *c* adsorbed on mercaptoundecanol monolayer electrodes, J. Electroanal. Chem. 564 (2004) 45–52.
[26] S.G. Sivakolundu, P.A. Maubrouk, Cytochrome *c* structure and redox function in mixed solvents are determined by the dielectric constant, J. Am. Chem. Soc. 122 (2000) 1513–1521.
[27] M. Paoli, J. Marels-Wright, A. Smith, Structure–function relationships in heme proteins, DNA Cell Biol. 21 (2002) 271–280.
[28] P.F. Barbara, T.J. Meyer, M.A. Ratner, Contemporary issues in electron transfer research, J. Phys. Chem. 100 (1996) 13148–13168.
[29] H.B. Gray, K. Niki, W.R. Hardy, M.G. Hill, H. Li, J.R. Sprinkle, E. Margoliash, K. Fujita, R. Tanimura, N. Nakamura, H. Ohno, J.H. Richards, Coupling to lysine-13 promotes electron tunneling through carboxylate-terminated alkanethiol self-assembled monolayers to cytochrome *c*, J. Phys. Chem., B 107 (2003) 9947–9949.
[30] K. Niki, J.R. Sprinkle, E. Margoliash, Intermolecular biological electron transfer: an electrochemical approach, Bioelectrochemistry 55 (2002) 37–40.
[31] G.R. Moore, G.W. Pettigrew, Cytochromes *c*. Evolutionary, Structural, and Physicochemical Aspects, Springer-Verlag, Berlin, 1990.

[32] A.K. Bhuyan, R. Kumar, Kinetic barries to the folding of horse cytochrome *c* in the reduced state, Biochemistry 41 (2002) 12821–12834.
[33] A.P. Demchenko, in: Topics in Fluorescence Spectroscopy: Biochemical Applications, vol. 3, Plenum Press, New York, 1992.
[34] A.K. Bhuyan, J.B. Udgaonkar, Multiple kinetic intermediates accumulate during the unfolding of horse cytochrome *c* in the oxidized state, Biochemistry 37 (1998) 9147–9155.
[35] Y. Goto, Y. Hagihara, H. Daizo, M. Hoshino, I. Nishii, Acid-induced unfolding and refolding transitions of cytochrome *c*: a three-state mechanism in H_2O and D_2O, Biochemistry 32 (1993) 11878–11885.
[36] J. Lakowicz, Principles of Fluorescence Spectroscopy, 2 ed., Kluwer Academic/Plenum Publishers, New York City, New York, 1999, pp. 452–456.